Chapter 4

A nanoporous palladium(II) bridged coordination polymer acting as a peroxidase mimic in a method for visual detection of glucose in tear and saliva

4.1 Introduction

The tremendous research interest in nanoporous coordination polymers (NPCPs) is boosted by the technological and scientific applications in view of important innovations in producing unique materials. Attractively, huge research attainment focused in the vicinity of this significant scaffold because of their specific size, structural regularity, high porosity, high surface area, easy tunability and design ability in a great potential for various application [Pan et al., 2004; Tiwari et al., 2016]. The structure and properties of NPCP based on the geometry and coordination behavior of organic linker and metal center, with other secondary interactions, for example, hydrogen bonding and features unique arrangement with elegant properties [Akhbari et al., 2013]. In this regard, a proficient architecture–directing organic linker 4-amino-3-hydrazino-5mercapto-1,2,4-triazole (AHMT) is used to manufacture functionally modified NPCP as the diazole nitrogen, hydrazino and sulfur atoms make possible the coordination of metal ion with the organic linker and making it, useful for sensing, catalysis, and modification of electrode applications [Cheng et al., 2009] .The hydrogen bonds and π stacking direct towards a refined arrangement and specific orientation of these building blocks [Haedler et al., 2015]. The emergence of nanoporous coordination polymers (NPCPs) are prominant group of nanoporous materials with promising applications in the various fields of gas storage/adsorption, luminescence, fuel cells, selective catalysis, magnetism, separation, sensing and so on [Li et al., 2016].

In this context, this article reports thorough investigation on synthesis, characterization and intrinsic catalytic activity of AHMT-Pd, NPCP. AHMT–Pd NPCP was synthesized under optimal conditions at room temperature in the absence of any extra additives. The

concentration of reactant was optimized during the synthesis and product was selectivity monitored by several instrumental techniques. The Pd(II) ions coordinated to the sulphur and nitrogen atoms of organic ligand afford outstanding capacity intended for molecular-level modification of the internal pore architecture [Kuwamura et al., 2017] and the cavities of AHMT–Pd NPCP can generate biomimic active centers. Therefore, NPCP comprises the enormous advantages of using efficient enzyme mimetic for the valuable application.

Natural enzymes catalyze all biochemical reactions due to high specificity towards a substrate that makes highly catalytic active bio-enzyme; they have been used in the biomedical application [Nirala et al., 2017; Vinita et al., 2018; Li et al., 2016]. Among enzymes, peroxidases have unique properties to catalyze the oxidation reaction of H_2O_2 and use in the biomedical application [Dayakar et al., 2016]. However, horseradish peroxidase (HRP) is the most typically used enzyme in clinical diagnosis but restricted to use due to catalytic activity affected by a harsh condition that changes in pH and temperature along with high cost of preparation, purification and storage stability [Ellis et al., 2009; Nirala et al., 2015]. Presently, enzyme mimetic nanomaterials have been used for detection of glucose. Dhara et al. has been demonstrated electrochemical nonenzymatic sensing of glucose using advanced nanomaterials [Dhara et al., 2018]. Nasir et al. has been reported an overview on enzyme-mimicking nanomaterials for use in electrochemical and optical assays [Nasir et al., 2017]. Further improvement in sensing parameters still needed.

Nowadays, metal-organic frameworks (MOFs) have emerged as a promising material to develop novel artificial enzymes, because their uniform cavities can generate a high density of biomimetic active centers [Wu et al., 2015; Li et al., 2014]. To the best of our knowledge, there are very few reports on the applications of colorimetric detection

based on the enzyme-mimic catalytic activities of MOFs for application in glucose and H_2O_2 sensing [Ortiz-Gómez et al., 2018].

In this contribution, colorimetric glucose detection has been formulated based on highly efficient peroxidase active AHMT–Pd NPCP. The, enzyme mimetic activity of nanoporous coordination polymer has not been reported till date. AHMT-Pd catalyzes peroxidase substrate 3,3,5,5-tetramethylbenzidine in presence of H_2O_2 to produce blue-green color of TMB oxidation product. This colorimetric assay is a highly sensitive and selective for H_2O_2 and glucose, and can be utilized to fabricate portable test kit based on agarose hydrogel to reveal a visual platform for determination of glucose in complex human serum by the bare eye. Additionally, this colorimetric assay is simple and do not require an expensive instrumentation.

4.2 Experimental section

4.2.1 Chemicals and materials

4-amino-3-hydrazino-5-mercapto-1,2,4-triazole (AHMT), palladium salt ($PdCl_2$), glucose oxidase (GOx, 100 units.mg^{-1}), hydrogen peroxide, glucose, horseradish peroxidase (HRP) agarose, 3,3′,5,5′-tetramethylbenzidine (TMB), were bought from sigma Aldrich, USA). HRP and GOx were biological reagents, and the other reagents were of analytical grade. Aqua regia (3: 1, HCl–HNO_3) was used to clean the glassware after that rinse with ultrapure water and ethanol (Merck India). Each chemical is used as acknowledged devoid of additional purification. Human blood serum samples have been collected from the authorized hospital. Serum samples were arranged on the similar day of collection.

4.2.2 Instrumentation

The FT–IR spectra of the ligand AHMT and polymer AHMT-Pd were performed in the range of 3400 to 500 cm^{-1} on KBr disc and attained with Perkin- Elmer 783 spectrometer. Powder XRD of AHMT and AHMT-Pd were recorded by a Miniflex 600 diffractometer (Cu–Kα radiation, Kα =1.54056 Å, 3°/min scan rate) in the range 10° to 80°. UV–Vis was recorded by Epoch 2 microplate reader Biotech (USA) spectrophotometer in quartz cuvette of 1 cm optical path length. X–ray photoelectron spectrometer (XPS), used for the elemental analysis was executed by Kratos Analytical Instrument, Shimadzu, Amicus XPS, UK. High resolution scanning electron microscope (HR-SEM) measurements were performed with Nova Nano-SEM 450 FEI, Netherlands. HR-TEM, the Energy Dispersive X-ray and mapping were executed with FEI, TECHNAI G^2 20 TWIN (Czech Republic) electron microscope operating with 200 keV accelerating voltage on a carbon-coated copper grid modified with 5 µL of an ethanolic solution of the polymer. Thermal analysis was performed on Mettler Toledo (TGA/DSC 1 STARE System, Switzerland) at a heating rate of 10 °C min^{-1} in the inert atmospheric condition.

4.2.3 Experimental procedure for AHMT-Pd Synthesis

The AHMT solution (13.5 mM) was prepared in hot water, 50°C (in order to dissolve the AHMT) and $PdCl_2$ solution (11.3 mM) in ethanol. Then AHMT solution was addded dropwise into $PdCl_2$ solution with vigorous stirring for 15 h at room temperature and atmospheric pressure. A brown precipitate of AHMT–Pd nanoporous coordination polymer was formed. The resulting precipitate was filtered and then washed five times followed by water–ethanol mixture solution to eliminate the unreacted $PdCl_2$ and AHMT. After drying under vacuum at 35 °C the yield was 83%. (Figure 4.1)

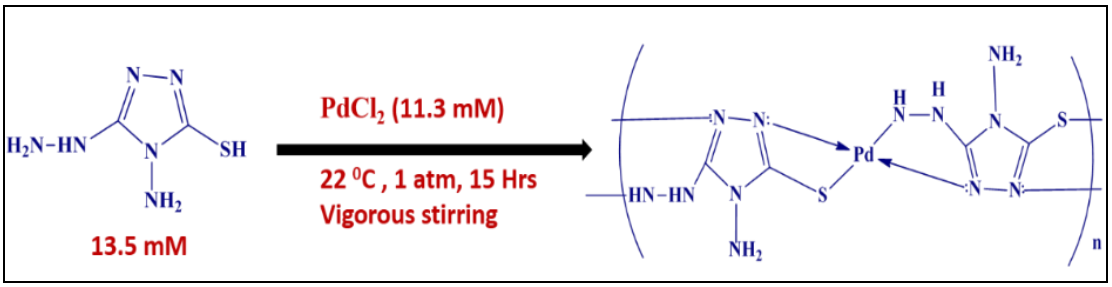

Figure 4.1 Reaction scheme for synthesis of nanoporous co-ordination polymer AHMT-Pd.

4.2.4 Colorimetric detection of glucose

A typical colorimetric detection of glucose was carried out as following procedure: 20 µL of GOx (5 mg·mL^{-1}) was added into various concentrations of glucose prepared in Phosphate buffer (0.1 M, pH 7.0) and incubated for 30 min at 40 °C to produce H_2O_2. There after 50 µL of AHMT-Pd (0.5 µg·mL^{-1}), 50 µL of TMB (1mM) with 300 µL Sodium acetate buffer (0.2 M, pH 4.0) were added to the above mixture and incubated at 40 °C for 30 min. The absorbance of the reaction solution was recorded at 652 nm.

4.2.5 Investigation of electrocatalytic activity of AHMT-Pd towards H_2O_2

Electrochemical detection of H_2O_2 was revealed as in brief, firstly we have taken 10 µL of AHMT-Pd (1 µg·mL^{-1}) cast over glassy carbon electrode (GCE). Then study the electrochemical response of formulated electrode in presence of different concentration of H_2O_2 by cyclic voltammetry in phosphate buffer (pH 7.0) (Figure 4.19).

4.2.6 Portable test kit for diabetes in real sample

A portable test kit was formulated for testing diabetes in a complex system. In briefly agarose (20 mg) was completely melted in 2 mL of hot water followed by stirring. After cooled down agarose solution to 40°C then 100 µL of aqueous solution of AHMT-Pd (20 µg·mL^{-1}) was added followed by 150 µL TMB (10 mM), and 100 µL GOx (10 mg·mL^{-1}). After gentle mixing of the solution, 150 µL of above aqueous solution was

transferred into the microcentrifuge tube (cap inside). Then dried at room temperature for 5 min to make a hydrogel in shaped and store the test kit at 4 °C for further sensing. The 30 µL serum sample was diluted to 900 µL using phosphate buffer (0.1 M, pH 7.0) and added to the portable test kit. Finally the cap of portable test kit was closed then inverted into upside down to permit the penetration of the reaction solution into the hydrogel and incubated for 30 min at 40 °C. The hydrogel color changed from colorless to blue-green, indicated the level of glucose in the real sample (Figure 4.2)

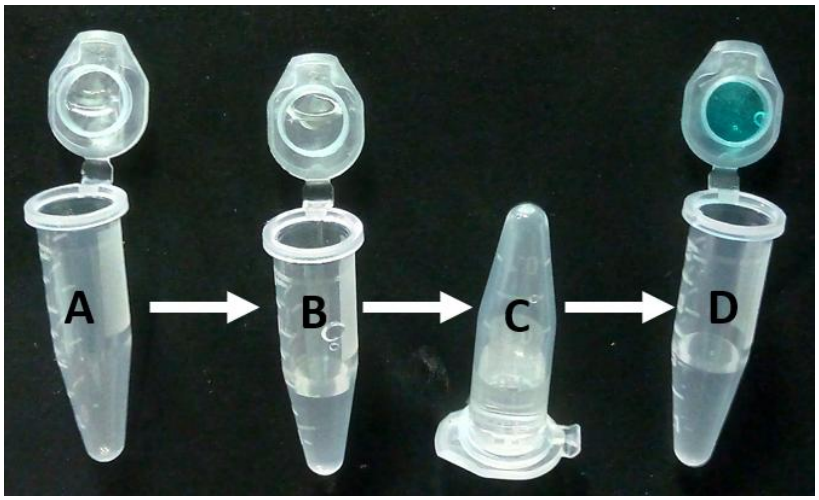

Figure 4.2 Portable test kit procedure for the detection of glucose in serum samples. (A) Opening the snap cap of the test kit (B) adding diluted serum sample solution to the test kit, (C) closing the snap cap and turning the test kit upside down before incubation at 40 °C for 30 min, and (D) turning the test kit upside down again and opening the snap cap to observe the color change of hydrogel (blue color in the hydrogel).

4.2.7 Determination of glucose in tear and saliva

The tear sample was collected through induced tearing with onion and saliva sample through psychological stimulation. The samples were boiled to denature the protein and centrifuged by Sorvall Legend Micro 21R Centrifuge, 24 x 1.5/2.0 mL Rotor with Click Seal Biocontainment Lid (Centrifuge force17, 108×g) for 10 min. Further supernatant was used for the analysis of glucose with reaction mixture of 30 µL saliva or tear, 50 µL TMB (10 mM), 50 µL GOx (10 mg·mL^{-1}), 7 µL AHMT-Pd (20 µg·mL^{-1}) and 30 µL

acetate buffer (0.2 M, pH 4.0). The absorbance of the reaction solution at 652 nm was recorded to know the glucose level. Standard addition method was adopted to know the glucose concentration by addition of known amount of glucose in the solution and LOD was calculated based on formula 3xStandard Deviation/slope of the curve.

4.3 Results and discussion

The AHMT-Pd NPCP is highly symmetrical molecule to facilitate the coordination sites for bonding and create a well–recognized structure based on multiple interactions, with the inimitable capability to form π stacking throughout the network. Pd(II) get coordinated through nitrogen and sulphur atoms of AHMT into an infinite arrangement of the polymeric chain structure. The structure of synthesized AHMT-Pd NPCP was investigated by FT-IR, XRD, UV-Vis, XPS, HR-SEM, TEM, EDS mapping and thermal analysis discussed later one by one.

4.3.1 Choice of Materials

Various types of system possess peroxidase like activities, for example gold nanoparticles, MoS_2 nanosheet, platinum nanoparticles, carbon nitride nanocomposites, vanadium disulfide nanosheet and so on. Though, noble metals nanoparticles are exploiting in disposable way, significant loss of noble metals occur [Chen et al., 2016; Huang et al., 2018]. Additionally uncontrolled aggregation, high costs, difficulty in separation low toxicity, porosity and thermal stability of several nanomaterials restricts their practical applications. Moreover, the uniform cavities of MOF can produce biomimic active centers. Therefore, AHMT-Pd coordination polymers are attracted due to their, high catalytic activity, low cost, high chemical and thermal stability. Furthermore porous AHMT-Pd provide good platform for sensitive detection of glucose because more enzymes are entrapped in porous cavity to increase catalytic activity.

Remarkable properties of AHMT-Pd coordination polymer as a peroxidase mimetic has been used to investigate colorimetric sensing of glucose.

4.3.2 Materials characterizations

For structural analysis, the FT-IR spectra of AHMT and AHMT-Pd were recorded in the region of 500–3400 cm^{-1} (Figure 4.3). The vibrational frequency at 3215 cm^{-1} is originated by υ ($NH\text{-}NH_2$) in AHMT which significantly attenuated towards 2974 cm^{-1} and broader in AHMT–Pd, emphasizing the linkage of exocyclic $NH\text{-}NH_2$ with Pd. Further, the S–H stretching appears at 2790 cm^{-1} in AHMT, get vanished in AHMT–Pd which supports the thiol group ionization and bonding of sulphur through the palladium atom. The peak at 1089 cm^{-1} in AHMT is allocated owing to an out of phase arrangement of N-N which get reduced to 1049 cm^{-1} in AHMT-Pd. The symmetric stretching (υ_s) at 1415 cm^{-1} and the asymmetric stretching (υ_{as}) at 1504 cm^{-1} of C=N are the most notable peaks of AHMT. The C=N band appears at 1382 cm^{-1} in AHMT-Pd. The reduced intensity of the C=N in AHMT-Pd support the coordination of the nitrogen atoms with palladium [do Carmo et al., 2015]. FTIR result shows the linkage of exocyclic $N\text{-}NH_2$ with Pd emphasizing the coordination of N-atom with Pd and bonding of sulfur with Pd atom.

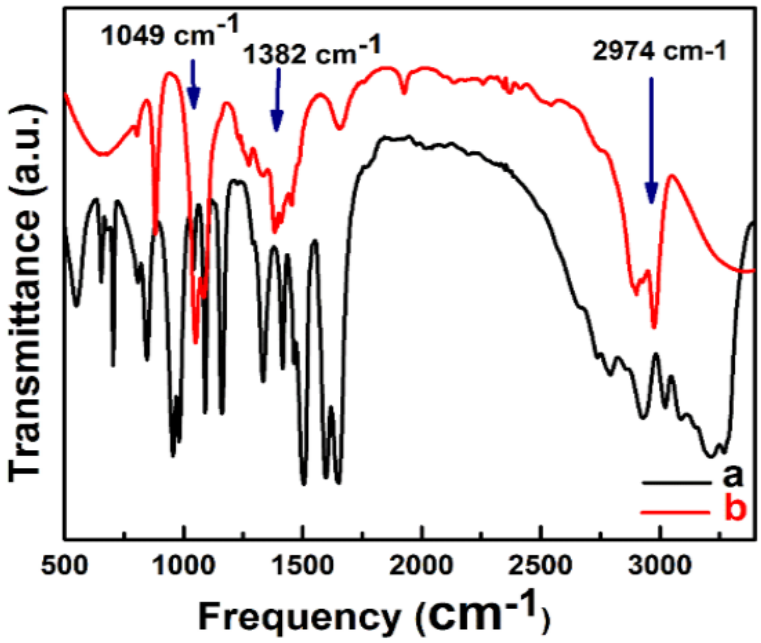

Figure 4.3 FT-IR spectra of AHMT (a) and AHMT-Pd (b).

The diffraction study of AHMT-Pd and AHMT were examined by XRD and also compared with Pd(0) acquired from JCPDS file CAS number 65-6174. AHMT-Pd shows a high amorphous environment due to polymeric nature [Tiwari et al., 2016] (Figure 4.4). Owing to the crystalline nature, AHMT and Pd(0) reveal strong diffraction peaks. It is noticeable from figure that the structural features of AHMT and Pd(0) are not present in AHMT-Pd. The amorphous nature of AHMT-Pd is furthermore investigated by SAED pattern of TEM elucidated later.

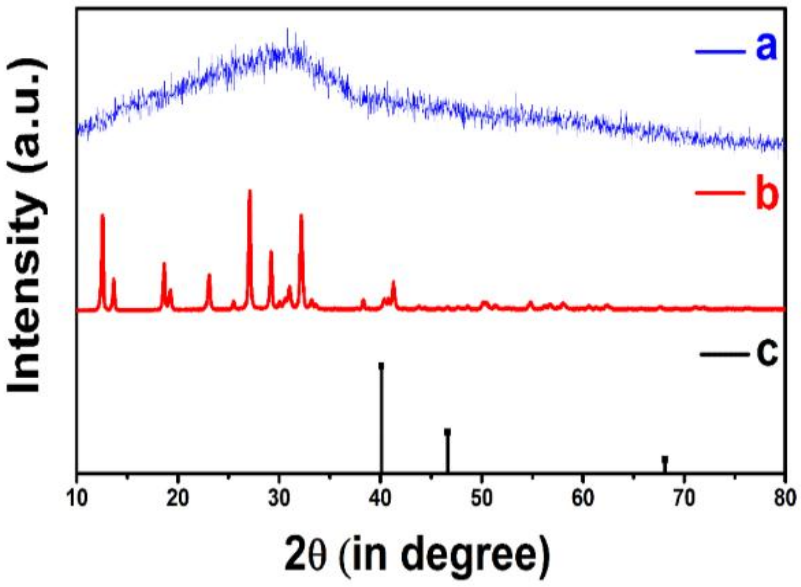

Figure 4.4 X-ray diffraction of AHMT-Pd (a) AHMT (b) and Pd (0) (c) obtained from JCPDS (CAS no. 65-6174.) file

The interaction of AHMT-Pd with respect to AHMT is depicted by the difference in absorption spectra (Figure 4.5). AHMT shows strong absorbance band near 360 nm, while AHMT-Pd exhibit feature centered absorbance band near 246 nm. The hypsochromic shift in the UV-Vis absorption spectra of AHMT-Pd is due to the interaction of AHMT with Pd.

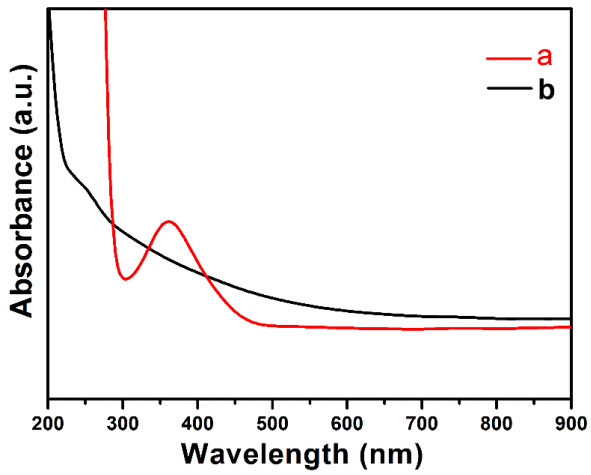

Figure 4.5 Absorption spectra of (a) AHMT and (b) AHMT -Pd.

The chemical nature of elements and oxidation state of Pd center in AHMT-Pd were investigated by the X–ray photoelectron spectroscopy (XPS). Peaks were fitted applying software XPS peak 4.1 (Figure 4.6). Two doublets are best fitted for the Pd(3d). The main binding energy of the peak at 342.5 eV is the distinguishing of $3d_{3/2}$ Pd(II) [Wang et al., 2013]. The binding energy at 337.2 eV is the characteristics of the $3d_{5/2}$ Pd(II) approve the oxidation state of metal in the polymeric structure. The deconvolution of N (1s) peaks provide 5 sets of singlet; the binding energy of the peak at 401.5 eV is corresponding to the endocyclic amine nitrogen (=N–) which also approves the bonding of imine nitrogen of =N- with palladium and resulting change towards high binding energy. The binding energy of 400.7 eV is credited to the –NH groups and supports the bonding of nitrogen of –NH with palladium. In addition binding energy at 400.1, 399.5 and 398.6 eV corresponding to C-N-C, C-NH- and $–NH_2$ sets of nitrogen [Daems et al., 2014]. The binding energy of the sulphur exhibits approximately at 162.7 eV corresponding to S (2p3/2). The variation of binding energy approves coordination of exocyclic sulphur with palladium atom. The C (1s) spectrum refers the binding energy at 286.4 eV and 285.3 eV and shows the proper fit comparable to N=C–N– and —N=C–S– bonding respectively [Lv et al., 2014].

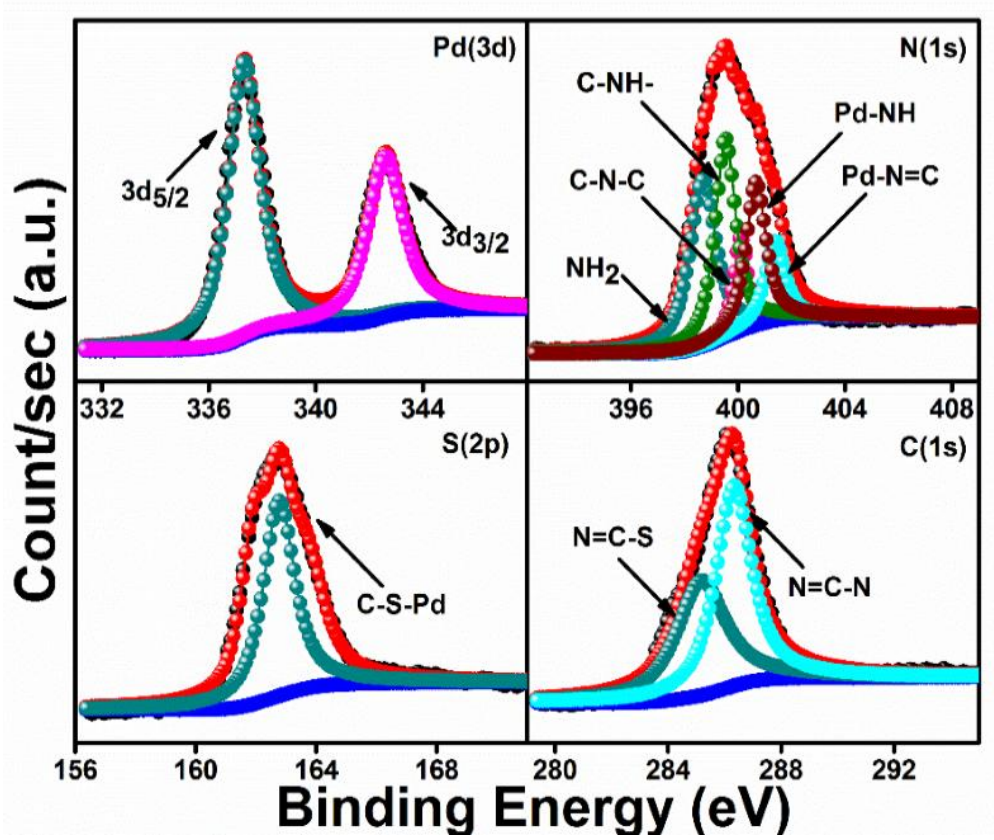

Figure 4.6 XPS spectra of AHMT–Pd for Pd (3d), N (1s), S (2p) and C (1s) regions.

The EDS mapping (Figure 4.9) depicted elemental composition of AHMT-Pd. Here, the overlap image reveals the homogeneous distribution of elements C, N, S and Pd indicating formation of compact polymeric chain throughout layers. Further the subsequent images (Figure 4.9) shows the mapping of the elements separately. The elemental analysis and morphology of AHMT-Pd are investigated by HR-SEM, TEM and SAED pattern as shown in Figure 4.7. The AHMT-Pd appears as porous nano globular shaped network structure (Figure 4.7a and 4.7b). Furthermore, irregular globules shape of the individual AHMT-Pd was also seen in TEM micrograph (Figure 4.7c and 4.7d). The extremely amorphous nature of AHMT-Pd network is also confirmed from SAED pattern (Inset of Figure 4.7d). The elemental composition of the AHMT-Pd is analyzed by EDX which exhibit the presence of Pd, N, S and C atoms in

the chosen area as shown in (Figure 4.8). On the basis of above characterization data the structure of nanoporous coordination polymer AHMT-Pd was anticipated (Figure 4.10). Here, the Pd(II) ions are associated with coordination sides of AHMT by nitrogen, and sulphur throughout the arrangement and the adjoining layers are stabilized by intermolecular hydrogen bonding and π stacking of aromatic system.

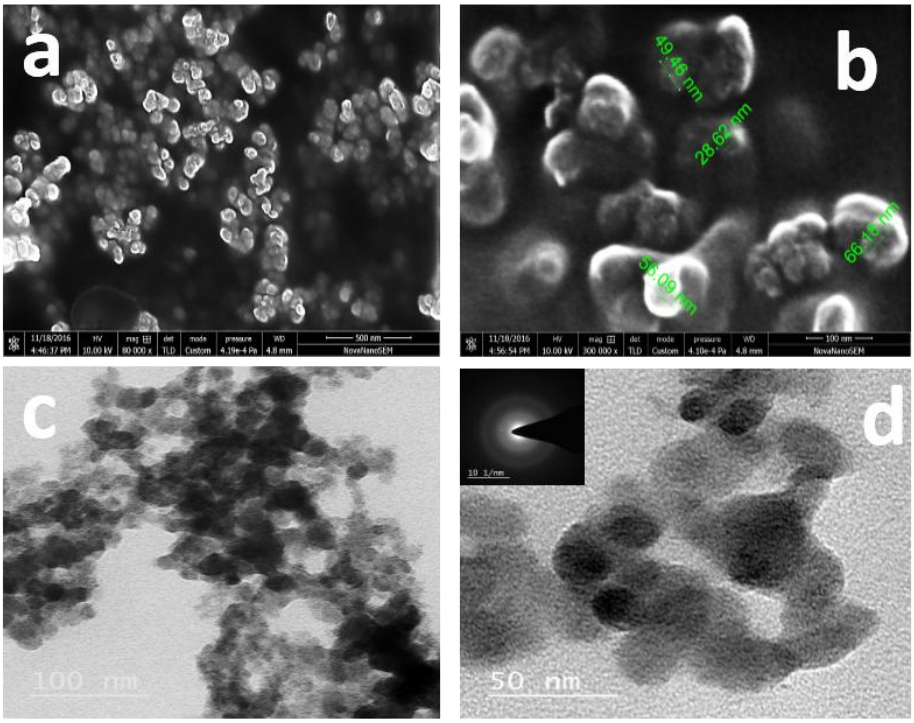

Figure 4.7 Structural morphology of AHMT-Pd (a) and (b) HR SEM, (c) and (d) TEM, inset of (d) corresponding SAED pattern.

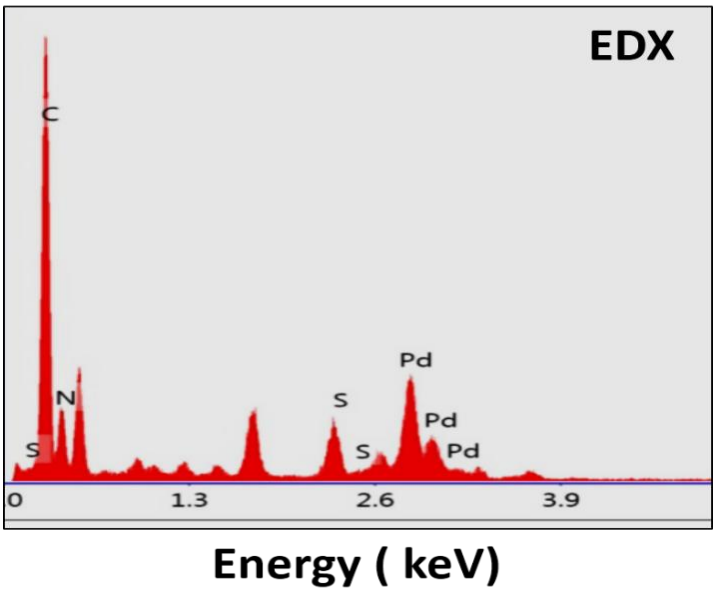

Figure 4.8 EDX of AHMT–Pd provided by HR TEM graph.

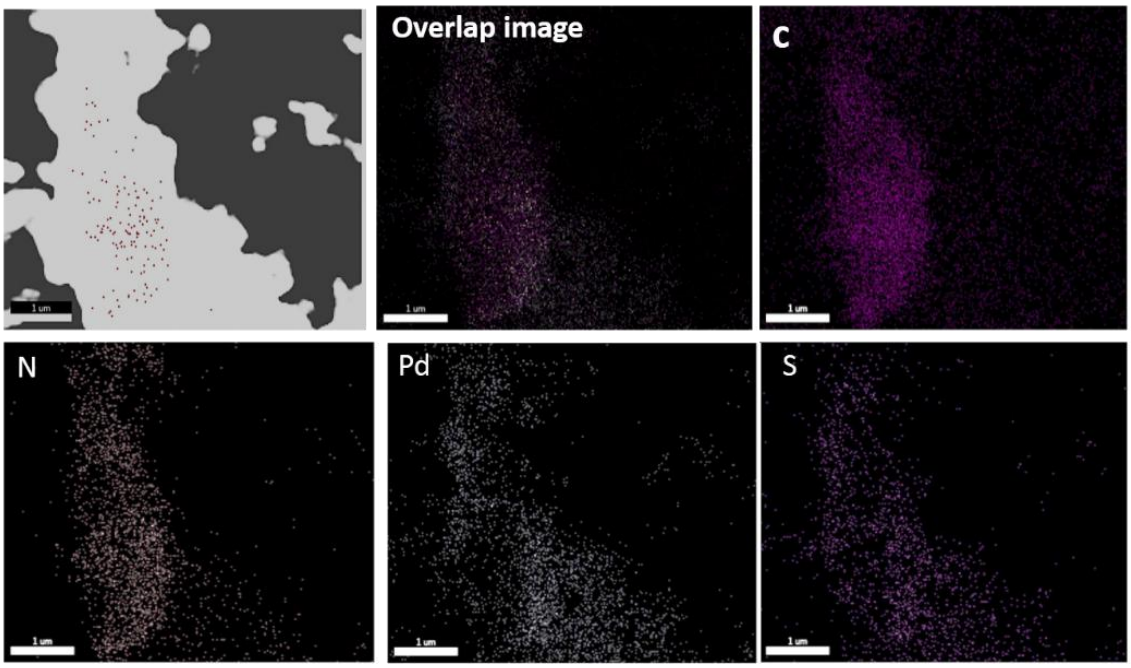

Figure 4.9 EDS Mapping of AHMT-Pd.

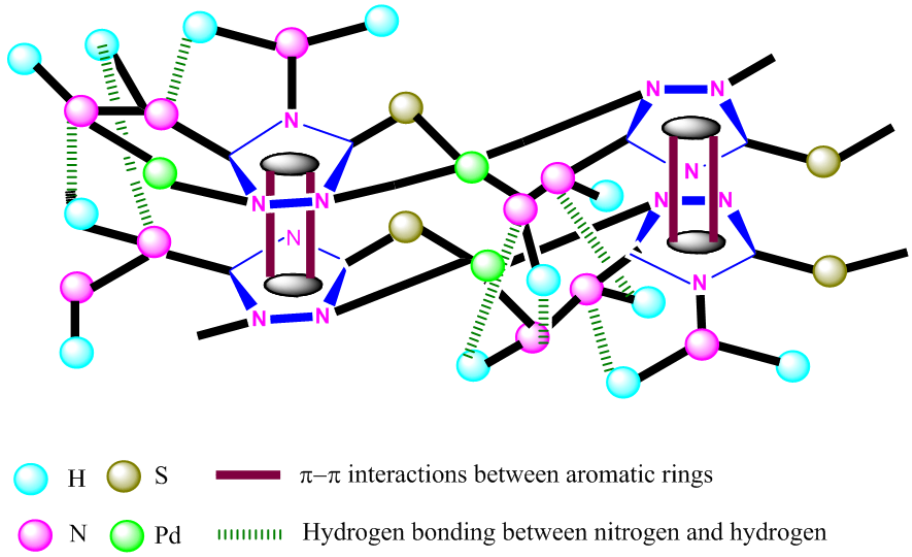

Figure 4.10 Structural network of AHMT-Pd.

Thermo–gravimetric analysis of AHMT-Pd was investigated under a nitrogen atmosphere for the study of activation energy and thermal stability. The thermal decomposition of AHMT-Pd was depicted by the thermal–gravimetric curve TGA/DTA (Figure 4.11). It reveals the thermal stability of AHMT-Pd up to 220 °C provided the thermally strong coordination polymer network. The first decomposition at 220 °C is because of the cleavage of coordination linkage. In addition, the slight degradation is observed in the 100°C temperature range due to uncoordinated molecules of water and further successive degradation are observed due to thermal breakdown of byproducts [Kaya et al., 2014]. DTA curve of AHMT–Pd shows an endothermic peak subsequent to the TGA graph. The activation energy of AHMT-Pd analogous to thermal degradation was calculated via Broido equation [Broido et al., 1969] as 15.79 kJ.mol^{-1} (Figure 4.12).

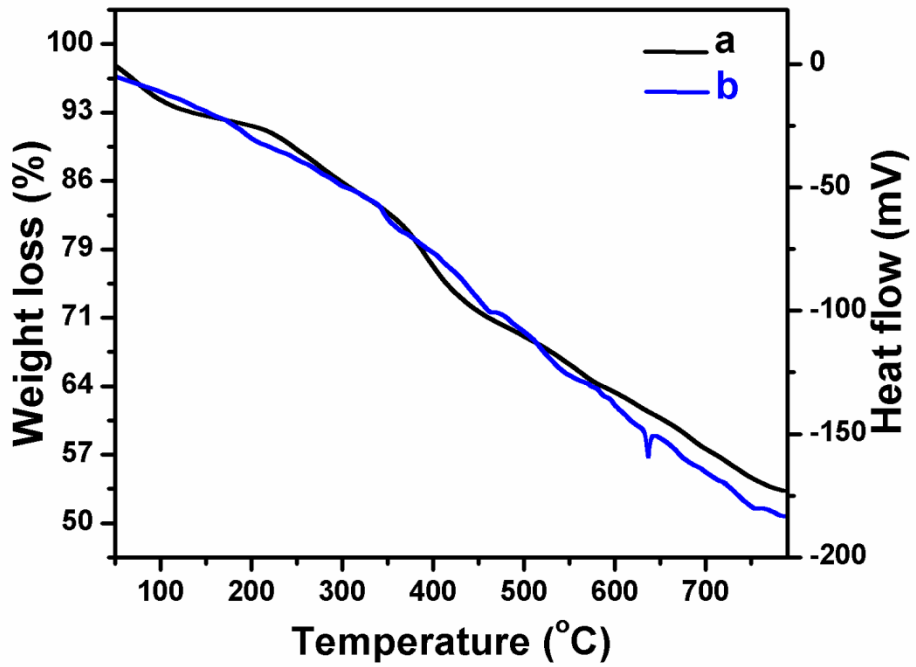

Figure 4.11 (a) TGA (left ordinate) and (b) DTA (right ordinate) plot of AHMT-Pd.

For the activation energy assessment Broido has proposed a method allied to thermal degradation. Activation energy (E_a) can be calculated by this equation (4.1).

$$ln\ [ln(1/Y)] = -(E_a/R)\ 1/T + constant \qquad \text{Eq. 4.1}$$

Here Y = $W_t - W_\infty / W_0 - W_\infty$

Y refers to the fraction of number of not degraded starting molecules; W_t is weight at time *t*, W_∞ is weight at infinite time (= zero) and W_o is the initial weight. Straight line is obtained from the graph of $ln\ [ln(1/Y)]$ *vs.* $1/T$ (Figure 4.12).

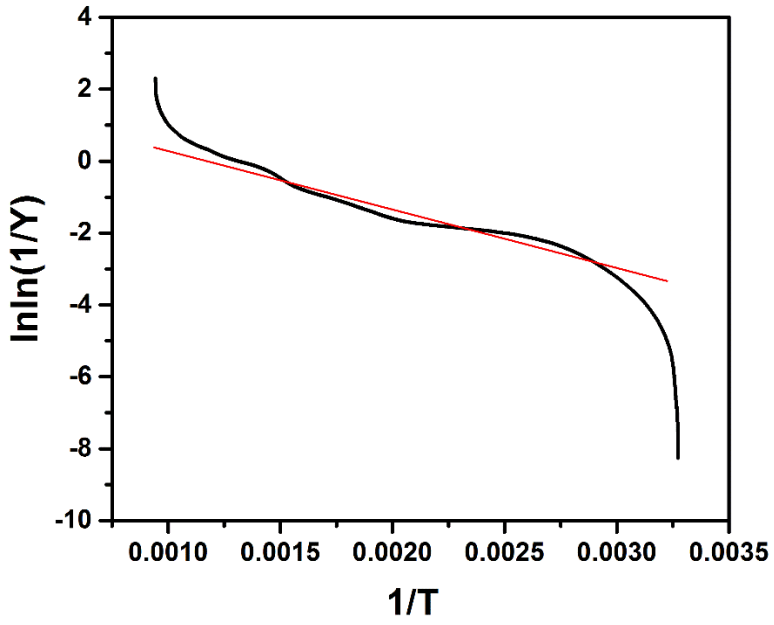

Figure 4.12 Plot of the Thermal activation energy for AHMT–Pd.

The activation energy for thermal degradation of AHMT–Pd is 15.79 kJ.mol^{-1} achieved from the slope of plot$(^{E_a}/_{R})$.

4.3.3 Investigation of peroxidase mimetic activity of AHMT-Pd

Peroxidase-like activity has been investigated through TMB oxidation in the presence of H_2O_2 catalyzed by AHMT-Pd system. The electron transfers to a catalyst AHMT-Pd from 3,5,3'5'-tetramethylbenzidine (TMB) with lone pair of electrons on amino group and characteristic peak appears at λ_{max} 285 nm for H_2O_2 reduction to either radical or ion formation [Wood et al., 1988; Liu et al., 2016]. The chromogenic substrate such as TMB oxidized in presence of H_2O_2 and catalyzed by AHMT-Pd which rapidly produces a green-blue color and shows significant absorbance peak at 652 nm of TMB oxidation and confirms the catalysis. The corresponding absorbance peak at 652 nm is used for the analytical study of hydrogen peroxide and products of TMB oxidation shown in Figure 4.13A. The change in typical absorbance peak of AHMT-Pd –TMB–H_2O_2 with a time was higher than TMB–H_2O_2 and AHMT-Pd –TMB system at 652 nm indicating

peroxidase mimetic activity of AHMT-Pd. The formulated catalytic mechanism of AHMT-Pd might be originated from increased electron density and mobility, due to fascinate transfer of lone-pair electrons from the amino groups of TMB to the AHMT-Pd [Lin et al., 2014]. Which confer the increase in Fermi level due to charge transfer, P-types nature resulting accelerates electron transfer from AHMT-Pd to H_2O_2 for the breakdown in H_2O and hydroxyl radicals. These hydroxyl radicals combine with TMB chromophore and make charge transfer complex with un-oxidized TMB shown in the blue colored product.

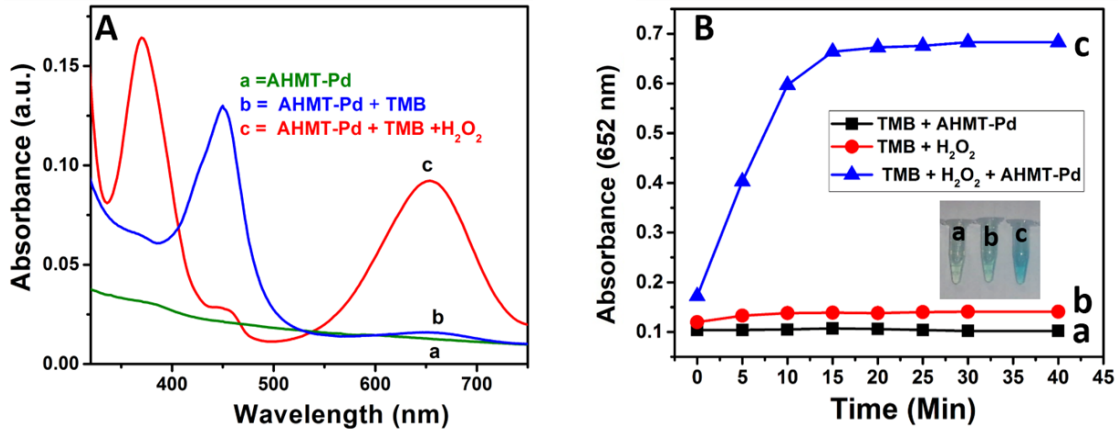

Figure 4.13 (A) Absorption spectra of various combinations of reaction systems (B) A typical absorbance peak changes with of TMB oxidation at 652 nm in different systems: AHMT-Pd, AHMT-Pd + TMB, TMB + H_2O_2, TMB + AHMT-Pd + H_2O_2. (Inset of B shows corresponding photograph of TMB oxidation products). AHMT-Pd (0.5 µgmL^{-1}), TMB (1mM) and H_2O_2 0.5 mM

TMB oxidation product shows characteristic peaks at 365 nm and 652 nm due to the formation of charge transfer complex with oxidized and parental un-oxidized TMB, resulting a blue color product. Thus H_2O_2 can be detected with variation in AHMT-Pd catalyzed intensity of this blue colored product. In typical cook's reaction, AHMT-Pd NPCP was added in TMB + H_2O_2 system, provided quick appearance of blue color confirming peroxidase activity of NPCP.

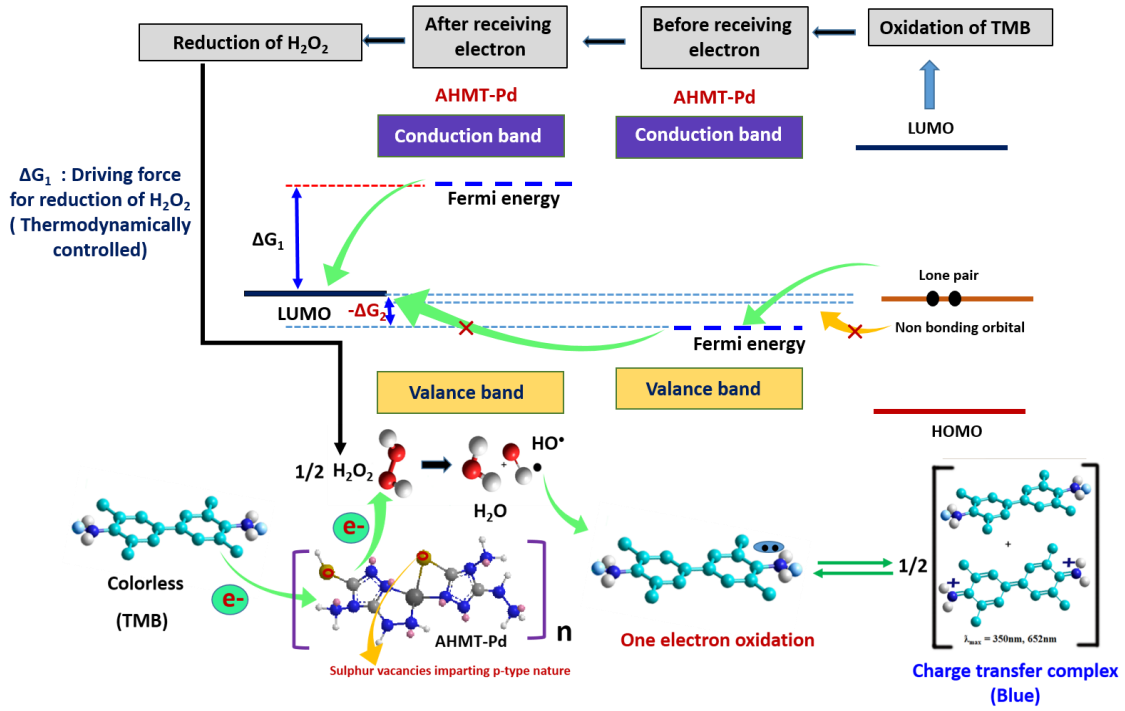

Figure 4.14 Possible mechanism for the electron transfer investigation and OH radical formation for production of colored TMB oxidation product in catalysis reaction.

The schematic (Figure 4.14) shows the investigation of electron transfer and OH radical's in catalytic TMB oxidation. The catalyst AHMT-Pd might be receiving electrons from TMB molecules due to the presence of nonbonding orbital (NBO) electrons, to significantly increased Fermi energy level for electron transfer from the catalyst to the LUMO of H_2O_2 by realizing redox potential is 0.38 eV [Wood et al., 1988] (Figure 4.14). TMB was significantly not showing oxidation product color (inset image, Figure 4.13B) in presence of H_2O_2 and experimentally proved by a negligible change in λ_{max} at 652 nm shown in (Figure 4.13B), (curve b). The higher band gap of AHMT-Pd (Figure 4.14) than TMB and H_2O_2 is a key factor for receiving electrons in TMB oxidation. However, in the case of our experiment, a significant absorption peak (λ_{max}) at 370 nm and 652 nm with the corresponding color was observed after addition of AHMT-Pd in H_2O_2 + TMB substrate shown in (Figure 4.13B) (curve c) due to charge transfer complex of TMB and also schematically represented in (Figure 4.14). AHMT-

Pd is a peroxidase active material which may have indorsed to it is a p-type nature due to the presence of sulphur vacancies [Xu et al., 2000]. The Fermi level energy increases due to facile electrons transfer from NBO of TMB to LUMO of H_2O_2 to reduce it and produce OH radicals. The Greater dynamic force of H_2O_2 reduction (high ΔG) requires the high energy of Fermi level of the catalyst for acceptance of electrons from TMB.

The mechanism of radical's formation in AHMT-Pd catalyzed TMB oxidation was proved by using OH radical scavenger (Ascorbic acid), $O_2^{\cdot}$ scavenger (Sodium Azide). In the case of ascorbic acids, the absorbance intensity get decreased (Figure 4.18). It reveals that TMB oxidation required OH radical to catalyze and produce color. However, In case of Sodium Azide absorbance intensity at 652 is not decreased.

4.3.3.1 Calculation of bang gap (Eg) of AHMT-Pd

The optical band gaps of AHMT-Pd nanoporous coordination polymer (Direct-gap semiconductor) might be virtually calculated by empirical formula given by Eq. (4.1).

$$(\alpha h\nu)^2 = A(h\nu - E_g) \qquad \text{Eq. 4.2}$$

Where A is a constant that depends on the transition probability, E_g is the optical band gap energy, h is the Plank constant and ν is the frequency.

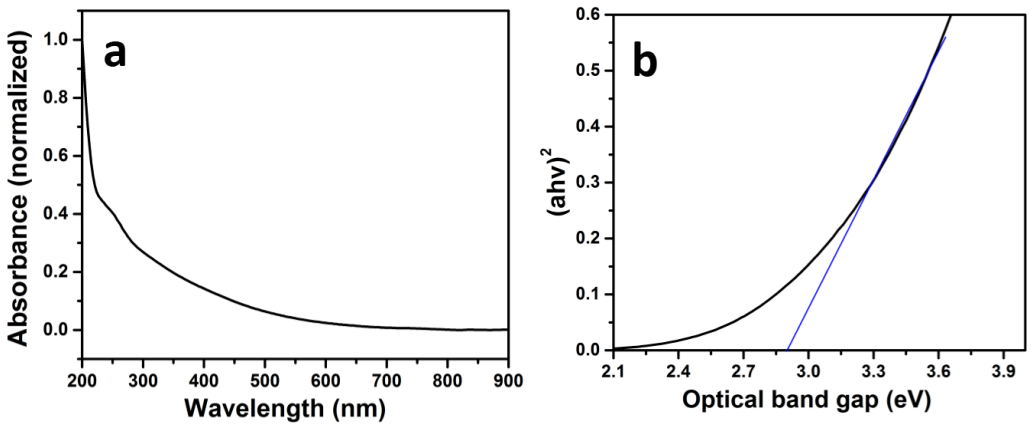

Figure 4.15 (a) The Normalized UV-Vis spectrum of AHMT-Pd, (b) $(\alpha h\nu)^2$ versus optical band gap achieved from equation.

The band gap of the AHMT-Pd NPCP was calculated by extrapolating a straight line in the plots of the $(\alpha h\nu)^2$ versus optical band gap energy to the $(\alpha h\nu)^2 = 0$ axis. By this method, the optical band gaps of AHMT-Pd can be calculated. It is admirable note that in UV-Vis spectrum the first absorption peak intensity should below 1.0 since to decrease the experimental error. When the transition probability value was assumed as 1, the simplified equation could be written as below by Eq. (4.3).

$$(\alpha h\nu)^2 = h\nu - E_g \qquad \text{Eq. 4.3}$$

Known function (Eq. 4.4)

$$h\nu = h\,C/\lambda = 1240/\lambda \qquad \text{Eq. 4.4}$$

Where, α is the absorption value in the UV-Vis spectrum, whereas λ is the detection wavelength. For example, Figure 4.15 (a) shows the normalized UV-Vis spectrum of AHMT-Pd. According to the above equation, Figure 4.15 (b) was attained by treating $(\alpha h\nu)^2$ as Y axis and $h\nu$ as X axis. The Eg (2.90 eV) could be estimated by extrapolating a straight line to the $(\alpha h\nu)^2 = 0$ axis in the plots of the $(\alpha h\nu)^2$ versus optical band gap energy.

4.3.4 Environmental effect investigation for catalytic activity of AHMT-Pd and HRP

The environmental effect for the catalytic activity of AHMT-Pd is investigated and compared with a natural enzyme HRP (Figure 4.16). The HRP catalytic efficiency is largely affected with pH and temperature (above 60 °C). The stunning catalytic activity of AHMT-Pd rather than HRP was experimentally observed at different temperature (25-80 °C) and pH (2.0-10.0) (Figure 4.16a, 4.16b). The catalysis of TMB in presence of H_2O_2 through AHMT-Pd is superior in acidic medium (pH 4.0) with good signal-to-

noise level. The AHMT-Pd explores higher catalytic activity at high H_2O_2 concentration (Figure 4.16c) and optimized to 0.5 µg·mL^{-1} for maximum catalysis (Figure 4.16d). Conclusively, the catalyst efficiency increases up to certain level with increasing catalyst and then decreases with the unavailability of active site.

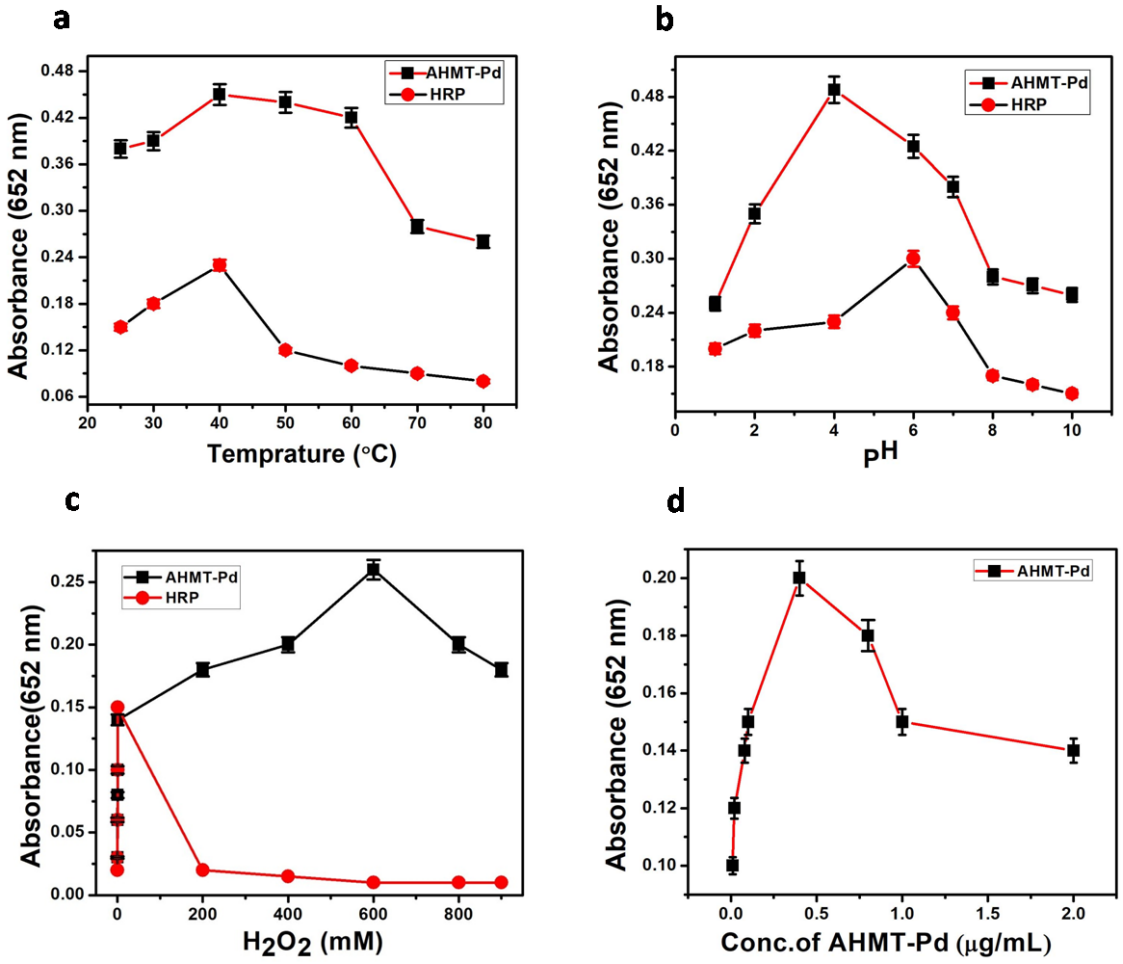

Figure 4.16 The peroxidase-like activity of AHMT-Pd and dependency on a) temperature, (b) pH, (c) H_2O_2 concentration and (d) AHMT-Pd concentration. Experiments were carried out at 0.5 µg·mL^{-1} AHMT-Pd in 1mL of 0.2 M acetate buffer with TMB (5 mM) as substrate. The H_2O_2 concentration was 0.5 mM at pH 4.0, the temperature was 40 °C.

4.3.5 Investigation of enzyme kinetics

To investigate the enzyme kinetic of catalytically active AHMT-Pd with TMB and H_2O_2, the concentration of TMB or H_2O_2 is fixed at a time. The initial rate of reaction is calculated by Beer–Lambert Law [Nirala et al., 2015]

$$C = A/\varepsilon b \qquad \text{Eq.4.5}$$

In the above equation, substrate concentrations are denoted by C, A is the absorbance of the reaction system, the thickness of the solution denoted by b. The concentration of the samples can be back calculated from its absorbance value from Eq.4.5 (The molar absorption coefficient (ε) for the TMB is 39,000 $M^{-1}cm^{-1}$) [Shi et al., 2011]. The enzyme kinetic parameters at different concentrations of the substrate are calculated with slopes of the absorbance changes with time (Table 4.1). In this case, Michaelis–Menten curves were developed for TMB and H_2O_2 where the maximum initial velocity (V_{max}) and Michaelis–Menten constant (K_m) are obtained from Michaelis–Menten equation.

Table 4.1 An illustration for calculation of initial reaction rate.

Absorbance	Time (sec)	The concentration of TMB-derived oxidation products (M ^{1}) (c=A/εb, where ε=39000 M^{-1} cm^{-1}, b=1 cm)	Average rate MS^{-1}
0.2	80	5.1×10^{-6}	
0.3	160	7.6×10^{-6}	
0.35	240	8.9×10^{-6}	4.4×10^{-4}
0.4	320	10.2×10^{-6}	
0.48	400	12×10^{-6}	

The better binding affinity of enzyme with substrates need smaller the value of K_m and greater V_{max} of enzyme offer good catalytic activity towards TMB substrates. In case of H_2O_2, the TMB concentration was fixed and the K_m value (0.4 mM) for AHMT-Pd was observed higher than HRP (Figure 4.17b), However in case of TMB, the H_2O_2

concentration was fixed and the K_m value (0.03 mM) for AHMT-Pd was found that smaller than HRP (Figure 4.17a). In this finding it is suggested that the number of active sites present in catalyst was fixed due to constant concentration of TMB and H_2O_2. The catalytic activity increases with increase active site numbers. The comparison for K_m and V_{max} values of AHMT-Pd with HRP and other nanomaterials provides lower K_m and higher V_{max} due to higher surface area allowing more interaction between glucose oxidase and TMB molecules. K_m and V_{max} of glucose with AHMT-Pd, and some other catalysts are tabulated (Table 4.2).

Table 4.2 Comparative table of steady state kinetics of various catalytic substrates and HRP though TMB oxidation.

Catalytic substrate	**K_m (mM)**		**V_{max} (10^{-6} s^{-1})**		**References**
	TMB	**H_2O_2**	**TMB**	**H_2O_2**	
C-Dots	0.039	26.77	3.61×10^{-8}	30.61×10^{-8}	[Shi et al., 2011]
MoS_2	0.525	0.0116	5.16×10^{-8}	4.29×10^{-8}	[Lin et al., 2014]
HRP	0.434	0.065	14.72×10^{-8}	5.65×10^{-8}	[Zheng et al., 2013]
Rh Nps	0.198	0.38	6.78×10^{-8}	2.41×10^{-8}	[Choleva et al., 2018]
AHMT-Pd	**0.03**	**0.4**	**8.5×10^{-6}**	**5.9×10^{-6}**	**Present work**

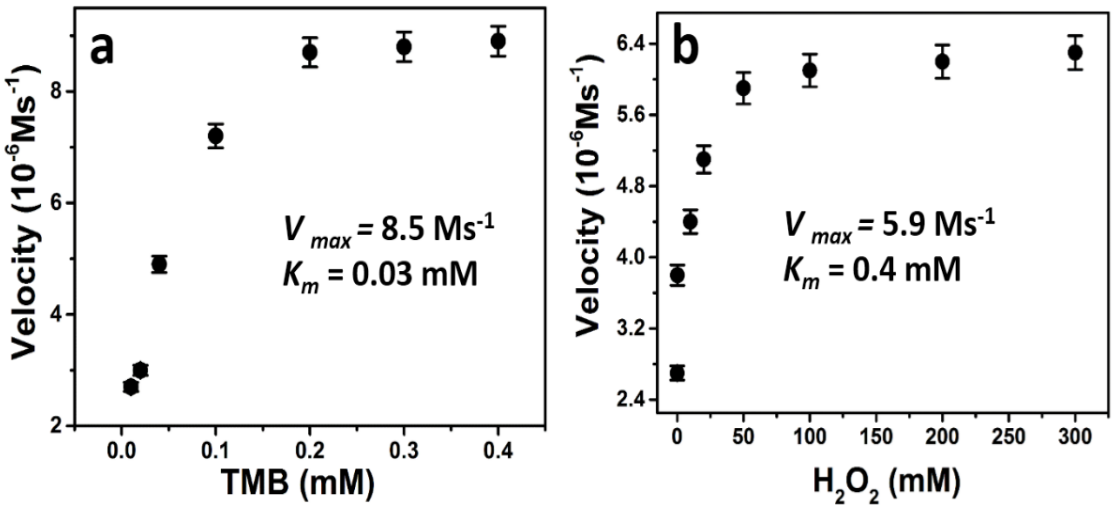

Figure 4.17 The enzyme kinetic K_m and V_{max} of AHMT-Pd toward TMB substrates (a and b). The analysis of reaction rate in presence of AHMT-Pd, 0.5 μg·mL^{-1} in 1 mL of 0.2 M sodium acetate buffer at pH 4.0, 40 °C. (a) The H_2O_2 concentration (10 mM) was fixed for AHMT-Pd and various TMB concentrations (b) Concentration of reactant TMB (0.1 mM) was fixed and the H_2O_2 was varied for AHMT-Pd.

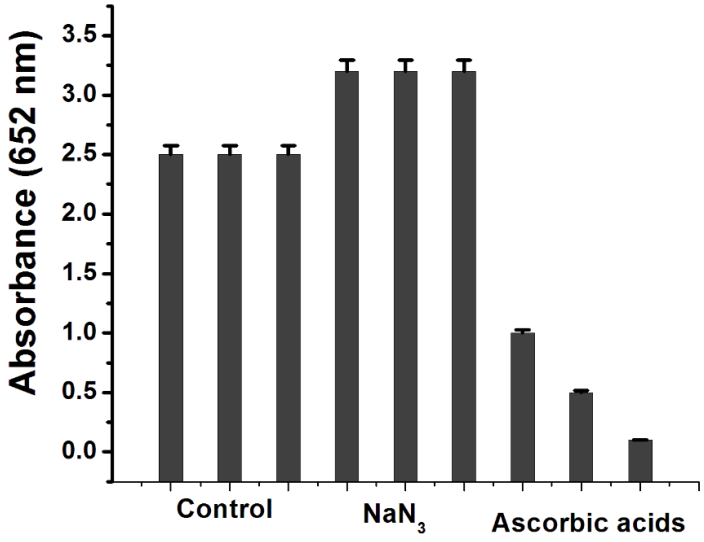

Figure 4.18 The catalytic reaction at the presence of different radical scavengers.

Procedures: 50 μL of AHMT-Pd (8 μg·mL^{-1}), 30 μL of TMB (5 mM), 100 μL sodium acetate buffer (pH 4.0, 0.2 M) and different amount of radical scavengers (5 μL, 10 μL and 15 μL) were mix together. The volume of the mixture solution was made up to 200 μL in water, after that 100 μL of H_2O_2 (0.1 mM) was added. Reaction was carried out

for 30 min at room temperature; the absorbance was recorded at 652 nm. The original concentrations of ascorbic acid and NaN_3 were 1 mM. The error bars stand for the standard error derived from three repeated measurements.

4.3.6 Electrochemical detection of H_2O_2 using catalytically active AHMT-Pd

The catalytic activity of AHMT-Pd was checked in detection of H_2O_2 and the remarkably increased current response with the variation of H_2O_2 concentration from 0 mM to 12 mM proves its catalytic proficiency. (Figure 4.19)

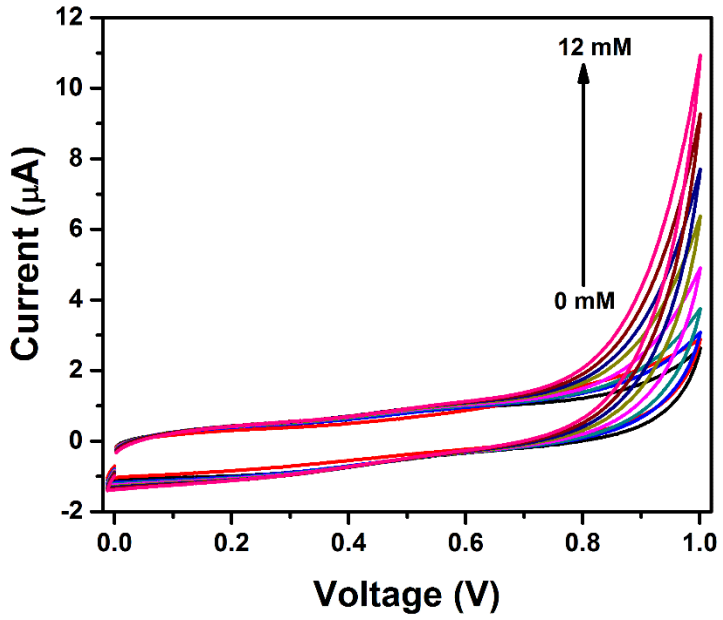

Figure 4.19 Electrochemical response of AHMT-Pd modified electrode catalysis of H_2O_2 in 0.1 M PBS, (pH, 7.0)

4.3.7 Colorimetric sensing of glucose with peroxidase active AHMT-Pd

Here the glucose oxidation is catalyzed by glucose oxidase (GOx) in the presence of oxygen to produce H_2O_2 which is required for AHMT-Pd catalyzed TMB oxidation. Therefore, TMB oxidized in presence of H_2O_2 which is came from the redox reaction of GOx and glucose and catalyzed by AHMT-Pd as shown in schematic (Figure 4.20).

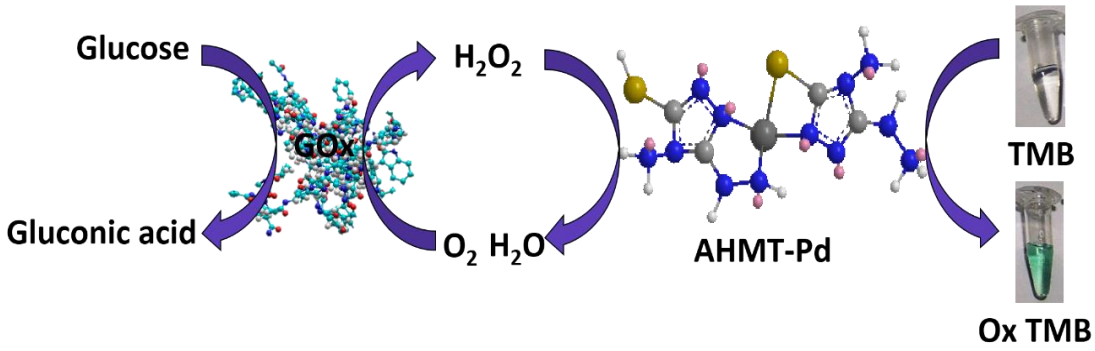

Figure 4.20 The schematic presentation of oxidation color reaction of TMB catalyzed by AHMT-Pd in presence of H_2O_2.

To demonstrate the proficiency of the designed colorimetric glucose detection system, different concentrations of glucose was monitored *via* the change in absorbance spectra which shows increased absorbance with increased glucose concentration (Figure 4.21a). It is observed that the designed catalytic system AHMT-Pd can detect minimum concentration (47 nM) of glucose (Figure 4.21b) and LOD was calculated 0.047±0.011µM (3xStandard Deviation/slope). The designed system is compared with various catalytic systems already reported which results that the designed system shows superior detection limit (Table 4.3).

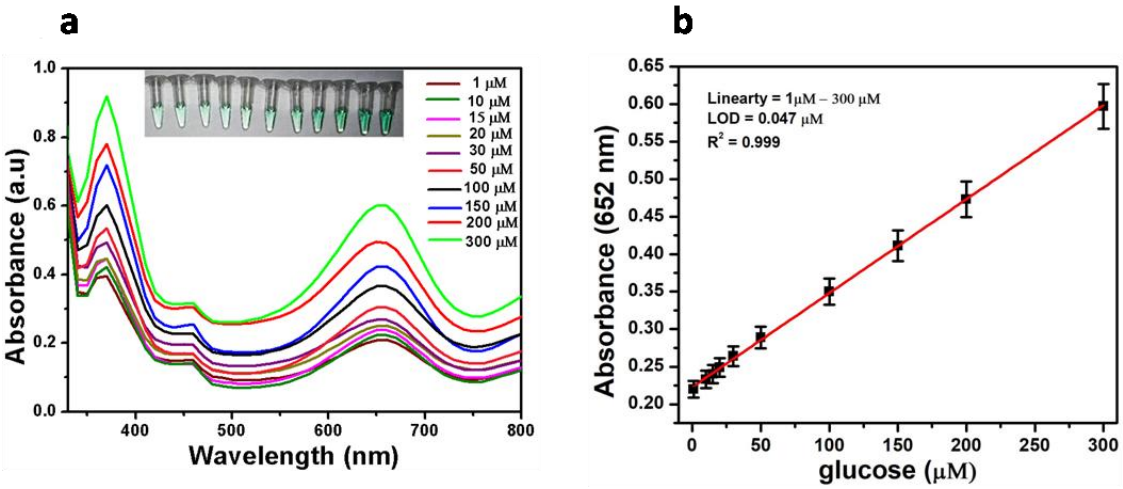

Figure 4.21 (a) UV-Visible spectra of a mixture of AHMT-Pd + TMB + GOx with different concentration of glucose (1µM, 2, 10, 15, 20, 30, 50, 100, 150, 200 and 300 µM) (b) corresponding calibration curve.

Table 4.3 Analytical figure of glucose detection based on various catalytic systems.

Catalytic system	**Method**	**Linear range (M)**	**Detection limit (µM)**	**References**
$ZnFe_2O_4$ Magnetic Nps	Colorimetry	1.25×10^{-6} - 1.87×10^{-5}	0.3	[Su et al., 2012]
VS_2 nanosheets	Colorimetry	5.0×10^{-6} - 2.5×10^{-4}	1.5	[Huang et al., 2018]
$Cu_2(OH)_3ClCeO_2$ nanocomposite	Colorimetry	0.1×10^{-3} - 2.0×10^{-4}	50	[Wang et al., 2015]
Magnetic Fe_3S_4 Nps	Colorimetry	2.0×10^{-6} - 100×10^{-6}	0.16	[Choleva et al., 2018]
Rh NPs	Colorimetry	5×10^{-6}- 125×10^{-6}	<0.75	[Choleva et al., 2018]
WS_2 nanosheets	Colorimetry	5.0×10^{-6}- 3.0×10^{-4}	2.9	[Lin et al., 2014]
AHMT-Pd	Colorimetry	1.0×10^{-6} 300×10^{-6}	0.047	Present work

4.3.8 Repeatability and reproducibility of the designed colorimetric system

The designed system is validated for reproducibility test by repeating experiments five times under same set of conditions and performing both in same day after 0, 3, 6, 9 and 12 h interval and inter-day after 1, 2, 3, 4, 5 days for the detection of glucose in the range 1 µM to 300 µM. Figure 4.22a and Figure 4.22b shows the good reproducibility for intra-day and inter-day glucose detection. The reproducible results have validated the efficient HRP mimetic potential of AHMT-Pd.

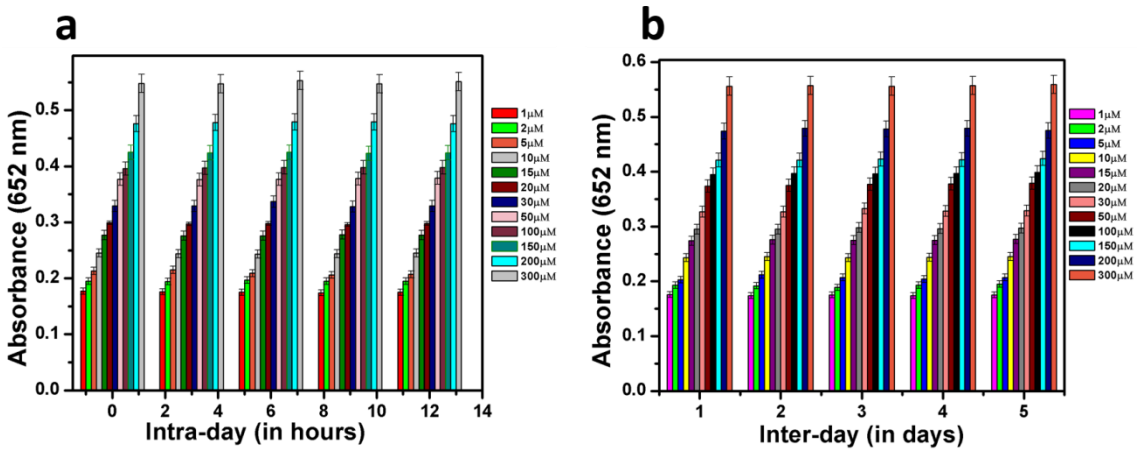

Figure 4.22 (a) Intra-day and (b) inter-day repeatability test result of AHMT-Pd (0.5 µgmL^{-1}) mediated detection of glucose (concentration range 1 µM - 300 µM). The error bar represents the standard deviation of triplicate measurement.

4.3.9 Selectivity and Interference Study

Designed system shows high specificity/selectivity towards glucose detection based on AHMT-Pd catalysis system. The selectivity was recorded in presence of interference like ascorbic acid, cysteine, uric acid, urea, cholesterol sucrose and fructose. The interference study was executed with mixture of fix glucose concentration (100 µM) and different interference e.g. 5 mM for urea, uric acid, ascorbic acid, cysteine, cholesterol, sucrose and fructose (Figure 4.23). AHMT-Pd system shows high selectivity (Figure 4.24) and good repeatability (Figure 4.24) towards glucose detection as evident from figure.

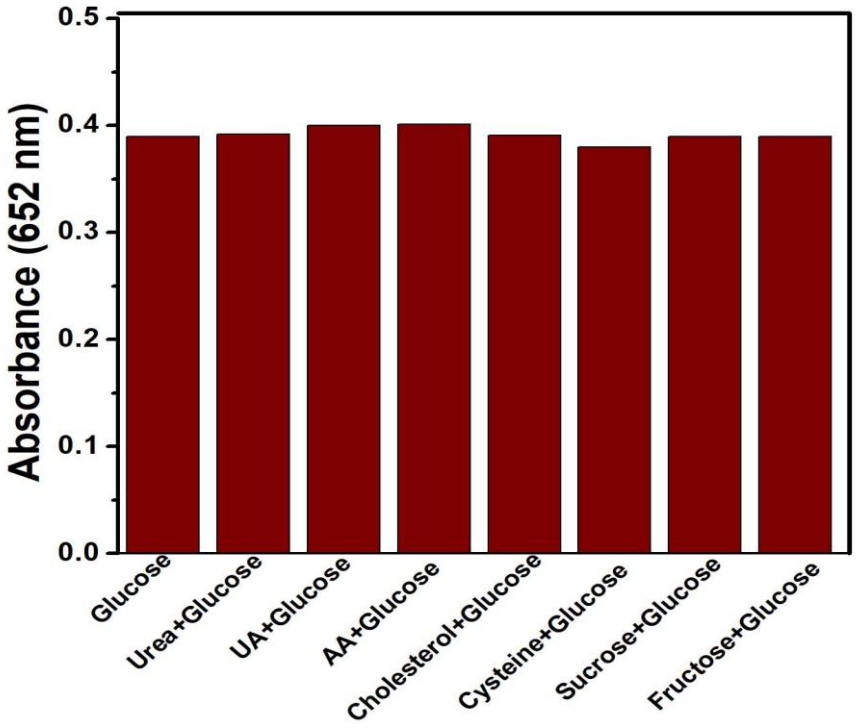

Figure 4.23 The catalytic reaction at the presence of different interferences.

Interference study was carried out as following procedure: Prepare the solution of glucose (100 μM) and different interferences (5 mM). 20 μL of GOx (5 $mgmL^{-1}$) was added into mixture solution of glucose and various interferences (urea, uric acid, ascorbic acid, cholesterol, cysteine, sucrose and fructose) prepared in Phosphate buffer (0.1 M, pH 7.0). There after 50 μL of AHMT-Pd (0.5 $\mu g \cdot mL^{-1}$), 50 μL of TMB (1mM) with 300 μL Sodium acetate buffer (0.2 M, pH 4.0) were added to the above mixture.

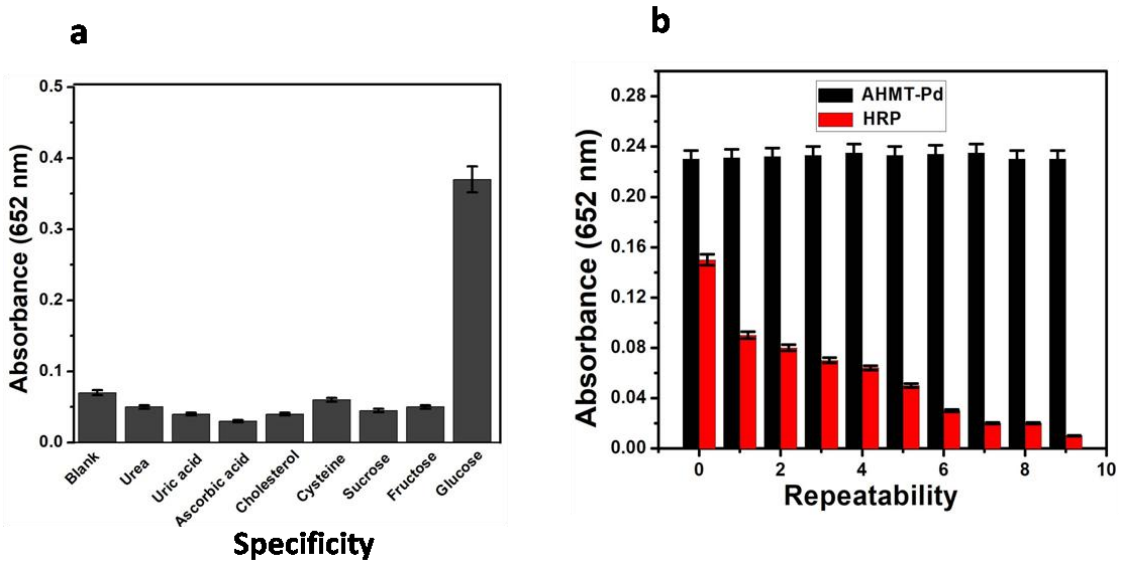

Figure 4.24 (a) Specificity of method for glucose detection. Specificity checked in 0.5 mL of 0.2 M sodium acetate buffer (pH 4.0) with TMB (1 mM), 0.5 μgmL^{-1}, AHMT-Pd and 1 $mgmL^{-1}$, glucose oxidase. (b) Ten times repeated experiments for glucose detection with AHMT-Pd (0.5 μgmL^{-1}), (1 mM) TMB solution and measurement in same set of reaction condition with GOx (1 $mgmL^{-1}$) and (0.1 mM) glucose. The error bars represent the standard deviation of three-time measurements.

4.3.10 Visual detection of glucose in serum sample by portable test kit

In order to prove the concept, the quantification of glucose was executed in complex systems of blood samples. A portable test kit is designed for visual detection of glucose level in serum through agarose hydrogel. In brief, 30 µL of serum sample was diluted to 30 times with pH (0.1 M, pH 7.0). The detection results of glucose in serum samples were shown in Figure 4.25. The hydrogel color changes from colorless (blank) to yellow-green in the normal range of glucose in a serum sample (2-5 mM) and further exceeding concentration cause color change from yellow-green to blue–green (8-12 mM) indicating the diabetic person. The designed portable test kit was applied to the visual detection of glucose in real serum samples without any expensive instrumentation. This method is free from any complex matrix effect of the blood sample and the results agree well with those obtained using the conventional Auto analyzer method (based on enzymatic reaction) (Table 4.4).

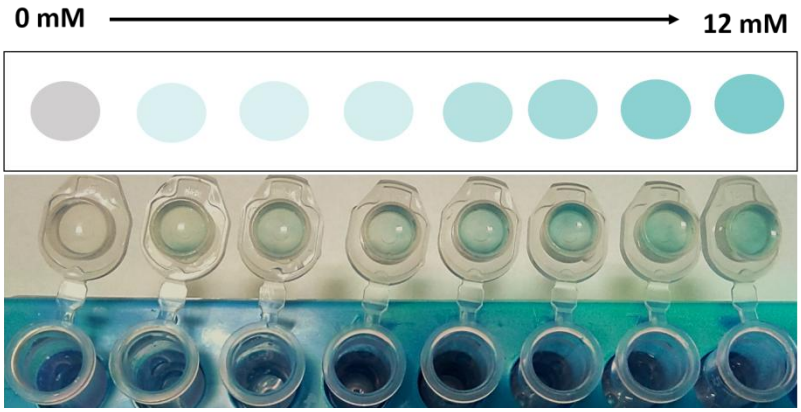

Figure 4.25 Human serum glucose level and corresponding typical colorimetric chart (from left to right: 0, 2, 4, 5, 8, 10, 11, 12 mM) (top); the hydrogel color change in presence of various concentrations of glucose in human complex system (opening the snap cap).

Table 4.4 Glucose determination in serum, tears and saliva samples.

S. No.	Auto-analyzer method (mg/dL) [a]			Proposed method (mg/dL) [b]			Relative Error (%)		
	Serum	Tears	Saliva	Serum	Tears	Saliva	Se	T	Sa
Sample 1	100	7.2	3.6	96 ±0.01[c]	7.0±0.01[c]	3.4±0.01[c]	4	2.7	5.5
Sample 2	180	14.4	10.8	174 ±0.01[c]	14.0±0.01[c]	10.4±0.01[c]	3.3	2.9	3.7
Sample 3	210	18	14.0	200±0.01[c]	17.4±0.01[c]	13.6±0.01[c]	4.7	3.3	4.2

[a] The concentration of glucose in samples have been Analyzed by using conventional Auto-analyzer(Automatic Chemistry Analyzer EKSV-240, Biochemical Analysis System) based on enzymatic reaction (Institute of medical science, Banaras Hindu University, Varanasi.)

[b] The confidence level was 94.5 %.

[c] Number of samples = 3

4.3.11. Non-invasive glucose determination in tear and saliva samples

The normal glucose concentration in human tear and saliva are 0.1–0.6 mM and 0.008–0.21 mM [Liu et al., 2015]. The technique is explored in tear and saliva in order to proof concept of this detection method which gives the lower detection limit (0.047 µM) in buffer compared to the glucose levels in tear (0.061±0.012 µM) and saliva (0.091±0.02 µM).

The AHMT-Pd system exhibit excellent response for glucose detection in tear and saliva and evidence that results in tear is better than saliva (Figure 4.26) indicating higher glucose concentration in tear than saliva.

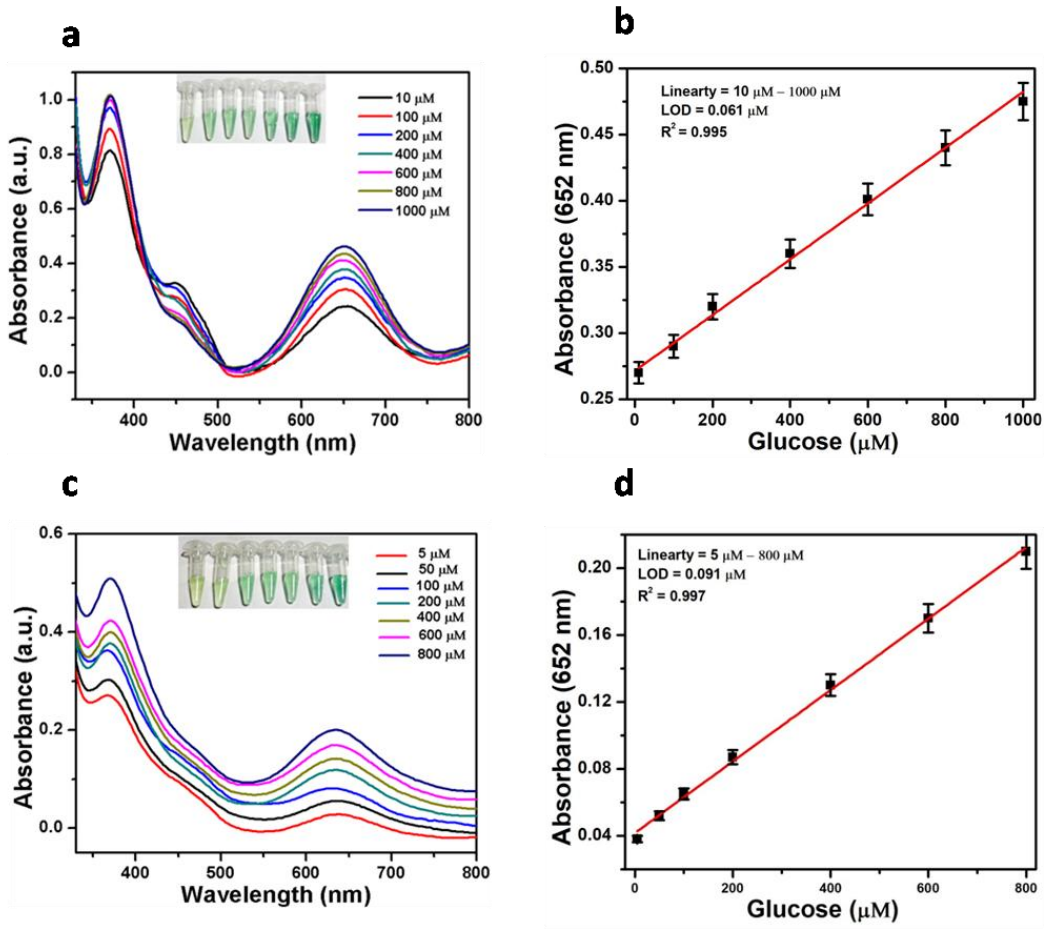

Figure 4.26 UV-Visible spectra of AHMT-Pd + TMB + GOx with different concentration of glucose (10 µM, 100, 200, 400, 600, 800 and 1000 µM) in tear (b) corresponding calibration curve (c) UV-Visible spectra of AHMT-Pd + TMB + GOx with different concentration of glucose (5 µM, 50, 100, 200, 400, 600 and µM) in saliva (b) corresponding calibration curve.

4.4 Conclusions

A nanoporous coordination polymer (AHMT-Pd) with the extended π conjugated system and high surface area is designed to facilitate fast electron transfer. It shows peroxidase-like activity to obey Michaelis–Menten kinetics. It catalyzes oxidation of TMB in presence of H_2O_2 to produce noticeable green blue color and the catalytic proficiency of AHMT-Pd depends on the concentration of catalyst, H_2O_2 concentration, temperature, and pH. Based on these finding, a portable test kit is formulated for visual assay of blood glucose level in the serum sample. The noticeable color change was observed from colorless to yellow–green for a normal range of glucose and blue–green indicates a diabetic person. The designed biosensing system is also able to determine glucose levels both in tear and saliva as a non-invasive assay. Moreover, the assay has potential to directly correlate color with the concentration of glucose in sample by Colorimetry test but the method can be used in biomedical application in environmental monitoring.